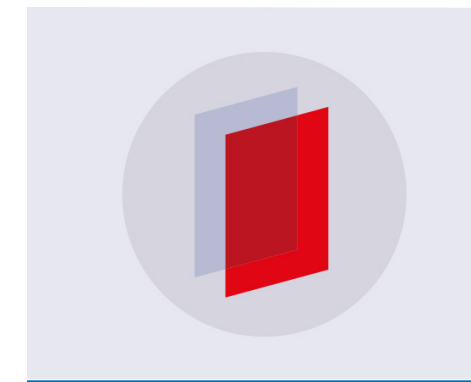
PAPER

Effect of swarm configuration on fluid transport during vertical collective motion

To cite this article: M M Wilhelmus et al 2020 Bioinspir. Biomim. 15 015002

View the <u>article online</u> for updates and enhancements.



IOP ebooks™

Bringing you innovative digital publishing with leading voices to create your essential collection of books in STEM research.

Start exploring the collection - download the first chapter of every title for free.

Bioinspiration & Biomimetics



1 October 2018

20 August 2019

ACCEPTED FOR PUBLICATION 11 September 2019

6 November 2019

PAPER

Effect of swarm configuration on fluid transport during vertical collective motion

M M Wilhelmus¹, J Nawroth², B Rallabandi¹ and J O Dabiri^{3,4}

- Department of Mechanical Engineering, University of California Riverside, 900 University Ave, Riverside, CA, 92521, United States of America
- Emulate, Inc., 27 Drydock Ave, Boston, MA, 02210, United States of America
- $Department of Mechanical \ Engineering, Stanford \ University, Stanford, CA, 94305, United \ States of \ American \ University, Stanford, CA, 94305, United \ States of \ American \ University, Stanford, CA, 94305, United \ States of \ American \ University, Stanford, CA, 94305, United \ States of \ American \ University, Stanford, CA, 94305, United \ States of \ American \ University, Stanford, CA, 94305, United \ States \ States \ University, Stanford, CA, 94305, United \ States \ States \ University, Stanford, CA, 94305, United \ States \ States \ University, Stanford, CA, 94305, United \ States \ States \ University, Stanford, CA, 94305, United \ States \ University, Univer$
- Department of Civil and Environmental Engineering, Stanford University, Stanford, CA, 94305, United States of America

E-mail: monicamo@engr.ucr.edu

Keywords: biomixing, swarm, collective motion, jellyfish, dispersion, ecosystem engineer

Supplementary material for this article is available online

Abstract

Understanding the hydrodynamics of self-propelled organisms is critical to evaluate the role of migrating zooplankton aggregations in sustaining marine ecosystems via the transport of nutrients and mixing of fluid properties. Analysis of transport and mixing during swimming is thus essential to assess whether biomixing is a relevant source of kinetic energy in the upper ocean. In this study, dilute swarms of the ephyral Aurelia aurita were simulated under different configurations to analyze the effects of inter-organism spacing and structure of a migrating aggregation on fluid transport. By using velocimetry data instead of numerically simulated velocity fields, our study integrates the effects of the near- and far-field flows. Lagrangian analysis of simulated fluid particles, both in homogeneous and stratified fluid, shows that the near-field flow ultimately dictates fluid dispersion. The discrepancy between our results and predictions made using low-order models (both in idealized fluid and within the Stokes limit) highlights the need to correctly represent the near-field flow resulting from swimming kinematics and organism morphology. Derived vertical stirring coefficients for all cases suggest that even in the limit of dilute aggregations, self-propelled organisms can play an important role in transporting fluid against density gradients.

1. Introduction

Fluid transport is an unavoidable byproduct of swimming. Yet, the fluid dynamic mechanisms available for self-propelled organisms to disperse fluid particles and eventually diffuse concentration gradients via mixing are not fully understood. Among the myriad of incentives to analyze transport and mixing due to swimming, one notable example is that of biogenic induced mixing. Also known as biomixing, this concept refers to the transport of carbon, nutrients, and oxygen attained by vertical migrations of zooplankton aggregations that has been hypothesized to be a source of intermittent diapycnal mixing in the stratified upper ocean [1].

Determining whether migratory species of zooplankton can indeed be considered ecosystem engineers has proved challenging [1, 2]. While in situ studies of swimming jellyfish have shown that self-propelled swimmers may achieve large scale transport via

Darwinian drift [3], coastal field microscale measurements in the vicinity of migrating krill aggregations have commonly detected low turbulence production, e.g. [4] and [5] (with one exception [6]). The difficulty of locating these events in the wild and concurrently identifying the contribution of migrating organisms to the energy distribution of the flow field (as in [7]) has prompted controlled lab-scale experiments, e.g. [8] and [9]. Although scaling experimental studies to yield representative marine conditions is rather impractical (i.e. only strong density gradients are feasible in a lab setting), important insights have been gathered, in particular concerning the length scales at which vertically migrating zooplankton aggregations introduce kinetic energy.

As explained in detail by Visser [10] and shown via dimensional analysis by Wagner et al [11], the length scale (*L*) at which kinetic energy is introduced during a migration event (assuming 3D isotropic turbulence) must be equal to or greater than the oceanic limit for biomixing to be relevant,

$$L \geqslant \sqrt{\frac{\varepsilon}{N^3}}$$
 , (1)

where ε is the turbulent kinetic energy dissipation rate, and *N* is the buoyancy frequency. Otherwise, all the work done by the vertically migrating aggregation is dissipated as heat by viscosity. Contrary to the hypothesis that the integral length scale during biomixing is commensurate with the body length of an individual swimmer, velocimetry studies triggering group behavior of A. salina on-demand via manipulation of phototactic signals found a pathway to large scale transport via the development of a Kelvin-Helmholtz instability during vertical migration in homogeneous fluid [9]. The follow-up study in a strongly stratified water column observed the same effect, in which large-scale recirculating regions adjacent to the migration event resulted in irreversible mixing [12]. It should be noted that an earlier experimental study by Noss and Lorke [8] reported incongruent results. In this study, however, group migration was not observed during the experiments (with the majority of the organisms solely swimming in the top and bottom parts of the tank). Moreover, it is not clear that hydrodynamic interactions between neighboring organisms during vertical migration were present as photographic records show migrating organisms swimming several body lengths apart from each other at any given time (in contrast to dense migration events captured in the wild [13]).

Analytically, the biomixing hypothesis has been analyzed by modeling self-propelled organisms both in Stokes and low-number-Reynolds flows (by applying Oseen's equation), e.g. [11, 14], and [15, 16], respectively. Under these approximations, linear equations of motion are recovered, and the time-averaged far-field flow of a low-Reynolds-number swimmer is modeled as the symmetric part of a point force dipole. Solutions obtained in this regime have allowed the rigorous analysis of the net momentum transfer at the wake, both in homogeneous and stratified fluids, and have provided first-order approximations to study the effect of ambient flow stratification [14] and turbulence on transport and mixing [15]. However, contradicting results with in situ jellyfish data [3] suggest that in order to precisely estimate transport due to a real swimmer both the near- and the far-field flows need to be considered in the analysis.

A more recent study comparing the long-adopted practice of modeling migrating species of zoo-plankton in the Stokes and Oseen limits with experimentally-derived drift measurements of zooplankton emphasizes the non-negligible role of inertia and swimming kinematics [17]. Also, direct numerical simulations of suspensions of so-called squirmers within an intermediate Reynolds regime highlight that disregard of the physical processes induced by inertial effects may incur in underestimating the efficiency of the biomixing process [18]. This point can be better illustrated by a simplified model of

migrating self-propelled organisms as steadily translating spheres in stratified potential flow [19]. Numerical tests comparing transport due to a single migrating organism and groups of swimmers with different configurations show an order-of-magnitude enhancement of fluid transport due to an increase of animal-fluid interactions when organisms swim in groups. Furthermore, even though inter-organism hydrodynamic interactions were absent from this model, these results suggest that the arrangement of swimmers within a group has an order-of-magnitude impact on net vertical fluid displacement.

Along with swimming kinematics, another often overlooked detail in numerical and theoretical models is that of morphology. A recent study comparing fluid advection under the Stokes and potential flow limits to that of freely swimming *Phylloriza* sp. with different morphologies found that differences in the wake structure inherent to the morphology and swimming kinematics of a particular species have a non-negligible impact on net vertical fluid transport [20].

Incorporating the near-field, swimming kinematics and morphology into numerical models of group migrations is a daunting task. To bypass this challenge, we adopted the technique proposed by Katija [20] to incorporate velocimetry data of free-swimming organisms in a numerical domain and simulate longer swimming trajectories by looping the data. We introduced many of these units within a prescribed configuration to model migrations of zooplankton aggregations, whereby the distance between adjacent swimmers was set sufficiently large to avoid hydrodynamic interactions. As a result, we can simulate vertical migrations of dilute zooplankton aggregations, and directly evaluate the effect of inter-organism spacing and thereby the structure of a migrating group on fluid transport (a parameter that is challenging to isolate in experimental studies). Furthermore, comparison of our results to first-order approximations of self-propelled swimmers both in potential [19] and Stokes flows allows us to examine the contribution of the near-field on fluid transport directly. It is important to note that conclusions drawn from our study are only relevant in the limit of migrating swarms with low organism density such that fluid dynamic interactions between adjacent swimmers are negligible. The results presented here can thus be considered a lower bound on fluid transport, complementing recent experimental observations of additional fluid dynamic mechanisms induced during vertical migrations of dense zooplankton groups [9, 12]. Finally, even though the focus of this study is the biomixing problem, the implications are potentially far-reaching given the observed growth of bio-robotics and the aim to employ them in a wide variety of applications (e.g. [21] and [22]). Whether the goal is efficient autonomous sensing, innovative biomedical devices, or new-generation autonomous vehicles, the analysis of transport and mixing due to propulsion has become increasingly important as well.

This paper is organized as follows. Section 2 provides a brief description of the experimental data for the swimming ephyra as well as of the processing of the flow field using particle image velocimetry (PIV). The rest of the section outlines the adopted numerical scheme. Section 3 presents fluid transport metrics for migrating groups of jellyfish with different swimmer configurations. Results are compared to the potential flow model by Dabiri [19] and to a low-order model in Stokes flow (details in the Appendix). Finally, in section 4, the contribution of the near-field to fluid transport is discussed and concluding remarks within the context of ocean mixing by swimming organisms are provided.

2. Methods

2.1. Flow field measurements

The flow generated by a vertically swimming ephyra of the scyphozoan jellyfish Aurelia aurita was measured using two-dimensional particle image velocimetry (PIV). Measurements were taken in water with constant salinity at room temperature. Prior to experiments, the water was seeded by adding and thoroughly mixing a concentrated stock suspension of test fluid and neutrally buoyant, silver-coated, hollow glass spheres of 13 μ m in diameter (Potter Industries Inc.). The particles were illuminated within a twodimensional plane generated using a 532 nm, 300 mW laser (Laserglow Technologies) and a plano-concave lens (FL = -4 mm). High-definition video of the freely swimming organism was acquired at 30 fps (exposure time of 1/60 s) using a Sony HDR-SR12 camcorder oriented perpendicular to the laser sheet [21].

Raw PIV images were processed to obtain a time series of instantaneous velocity fields. Consecutive image pairs were cross-correlated using Davis 9 (LaVision Inc.). Image interrogation was conducted via two multi-pass iterations of decreasing window size from 64×64 to 32×32 pixels with a 50% overlap. Post-processing of the velocity fields was achieved by applying a universal outlier detection scheme [23].

Vertical migrations of jellyfish swarms were simulated by assimilating the computed time series of instantaneous velocity fields onto a larger two-dimensional domain. The effects of the near- and the far-field flows were thus included in the analysis, bypassing the need to solve the non-linear Navier–Stokes equations. In the model, swimmers were set to translate vertically according to the measured vertical displacement of the centroid position of A. aurita (described in section 2.2). Similarly to recent work by Katija [20], continuity in the trajectories was ensured by considering velocimetry measurements corresponding to complete swimming cycles. From the acquired PIV data, a total of three complete power-and-recovery strokes were retrieved (refer to section 2.3). These were taken as the building blocks to simulate longer swimming trajectories. Vertically migrating swarms were simulated by introducing neighboring swimmers according

to a pre-determined configuration (as in [19]), under the constraint of zero overlap between adjoining flow fields.

2.2. Centroid identification

To accurately determine the centroid of the jellyfish at each time step, the raw PIV image sequence was analyzed (Adobe Photoshop Elements 9) to discern the contour of the jellyfish body from the background. The region encompassed by the contour of the organism was marked with white, and the uneven illumination of the image due to the reflection of the PIV particles was replaced with a uniform black background (figure 1). The centroid position was computed from the obtained black-and-white images using the regionprops command in Matlab. The average swimming speed of A. aurita was then calculated from the time series of the displacements $(4.24 \pm 0.01 \text{ mm s}^{-1})$. Considering the diameter of the bell as the characteristic length scale ($D = 7.3 \pm 0.02$ mm), the Reynolds number of operation of A. aurita (based on D) is Re = 30. It should be noted that the jellyfish was originally captured swimming towards a deeper vertical position (figure 1). The raw images were flipped in the vertical direction to simulate vertical migrations from a deeper region to a shallower one, which does not modify the generated flow field owing to the neutral buoyancy of the jellyfish (figure 2).

2.3. Cropping of the velocity field

On account of the near field flow generated by freeswimming A. aurita, the instantaneous velocity fields were cropped along a rectangular box of constant width and height (roughly twice the size of the organism). The vorticity (ω) generated by the ephyra as it propels forward is compact in a region close to its body; even as the contraction of the bell during the power swimming stroke $(1.3 \pm 0.05 \text{ Hz})$ results in vortex shedding [21]. Furthermore, given the low Reynolds number of the flow (Re = 30), the shedded vortex rings are hypothesized to persist for a short period of time such that interactions between swimmers are negligible. In the case of A. aurita this assumption is justified based on previous experimental studies by Dabiri et al [24] showing the cancellation of vorticity during subsequent contraction and relaxation of the bell, resulting in a reduced downstream propagation of the formed vortex rings. Hence, the instantaneous velocity fields were cropped such that ω is effectively zero outside of the cropping region (figure 3). The exact threshold was set at $\pm 0.2 \text{ s}^{-1}$, matching values at distances greater than four body diameters from the centroid of the organism.

A total of five complete swimming cycles were identified in the raw data, from which the first and last one had to be discarded due to the proximity of the body of the jellyfish to the top and bottom edges of the field of view of the camera. As a result, instantaneous velocity fields spanning the remaining three

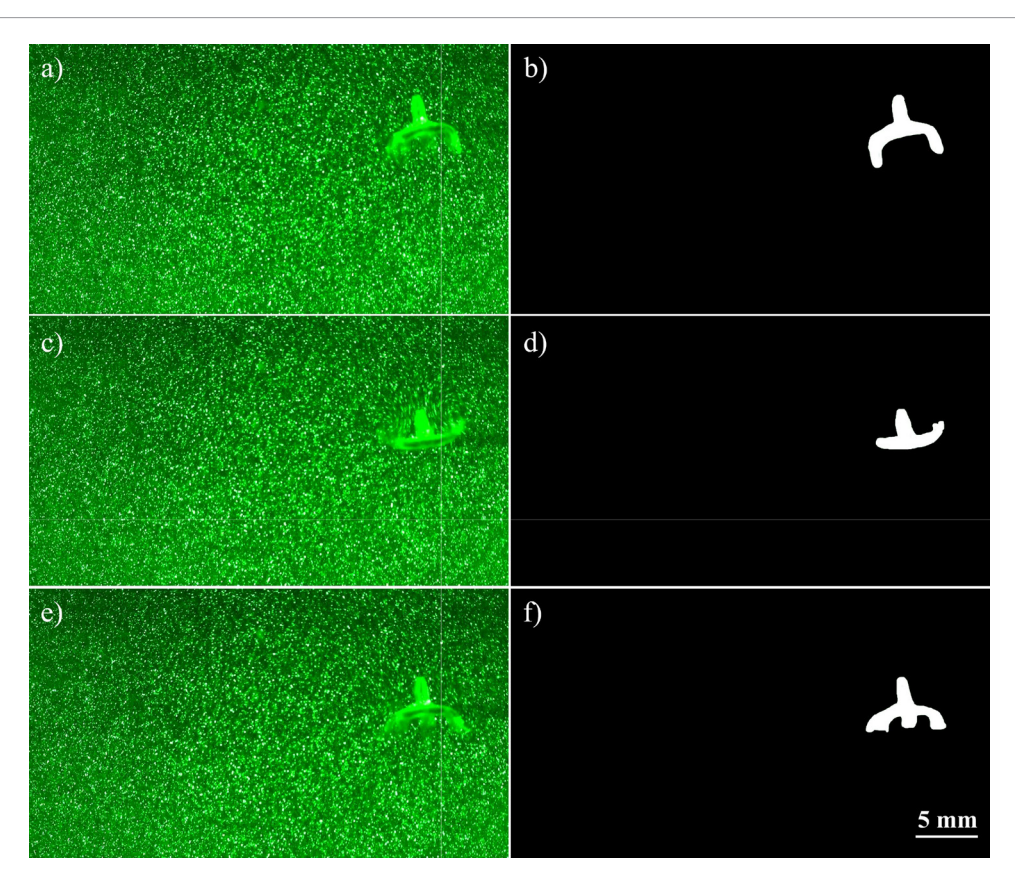


Figure 1. Animal contour detection. Image pairs show raw data ((a),(c),(e)) and their processed versions displaying the identified jellyfish contour ((b),(d),(f)) within different time steps. The time between consecutive images is $\Delta t = 0.27$ s.

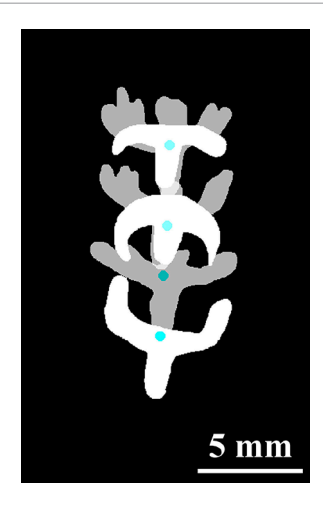


Figure 2. Centroid detection of *A. aurita*. An overlay of the body of the jellyfish (re-oriented to simulate a bottom-to-top migration) is shown at different instants ($\Delta t = 0.46\,\mathrm{s}$). The computed centroid position of the organism is indicated with a blue dot.

swimming cycles were cropped with respect to the centroid of the jellyfish. To this end, the velocity field was linearly interpolated such that the centroid position was included within the set of nodes of the velocity grid, with respect to which the crop box was defined.

2.4. Numerical experiments

The experimentally measured velocity data spanning three swimming cycles and spatially bounded by the extent of the near-body vorticity field constituted the elementary unit from which vertically migrating aggregations were constructed in our model. Boundary conditions were not imposed on the jellyfish body since this would artificially alter the measured velocity fields. The case of a single swimmer vertically migrating was analyzed along with three different configurations of jellyfish aggregations with swimmers migrating in line as well as in two- and three-column staggered formations (figure 4).

The vertical migration of jellyfish was modeled both in homogeneous ($N = 0 \text{ s}^{-1}$) and weakly stratified fluid environments ($N = 10^{-3} \text{ s}^{-1}$), with the last value being comparable to the average buoyancy frequency in marine environments [25]. To compare the results of our hybrid model to the idealized flow transport studies by Dabiri [19], the setup of the swarm migration cases was prescribed according to his model, which implements arrays of solid dragged spheres with momentum-less wakes to model the flow due to aggregations of steady self-propelled swimmers. The horizontal spacing between neighboring organisms was thus set to D/2, while the vertical distance between swimmers was greater than the maximum vertical particle displacement achieved by an individual organism swimming in homogeneous fluid, which resulted in a spacing of 8D (figure 4). Additional tests reducing both the horizontal and vertical distances between swimmers were conducted for all swimmer configurations (the former only in the limit of weakly

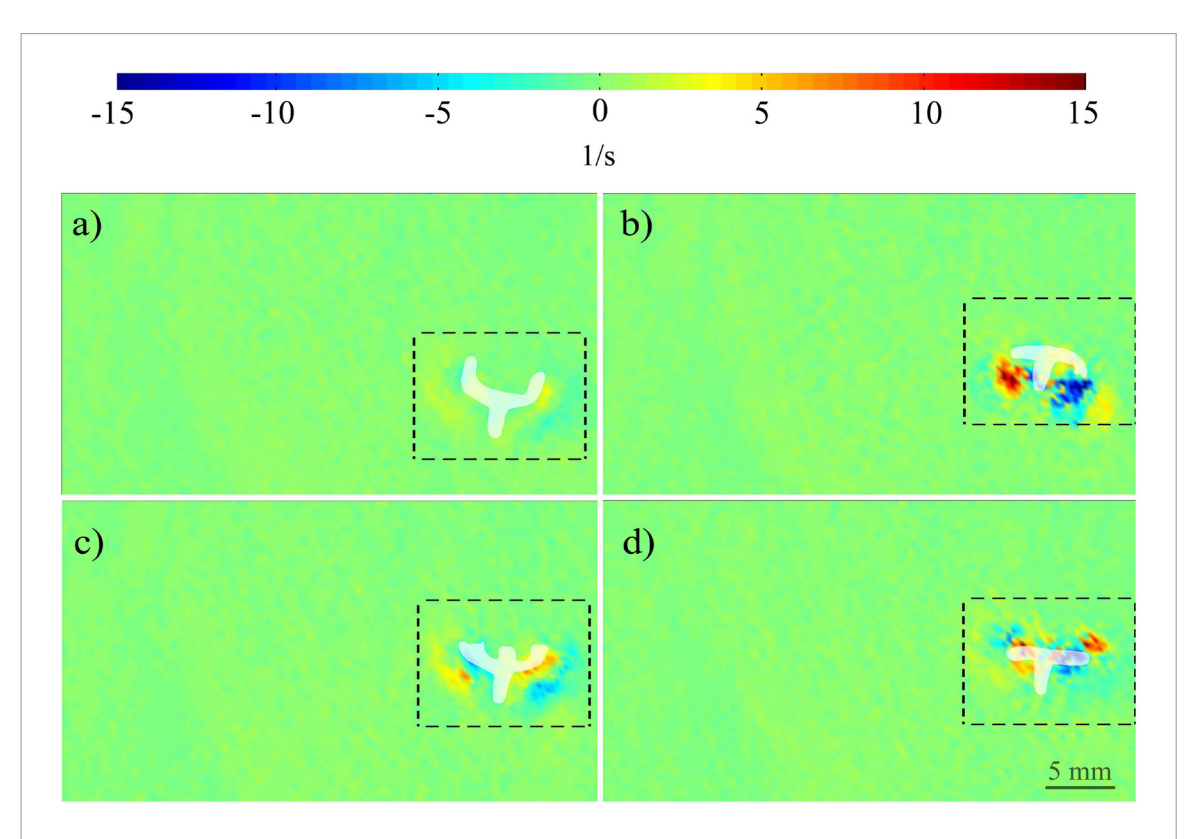


Figure 3. Vorticity field series during propulsion of *A. aurita*. The vorticity field during propulsion is shown for the complete camera field of view. The broken lines define the rectangular region used to crop the velocity fields at each instant. The time between images is $\Delta t = 0.27$ s.

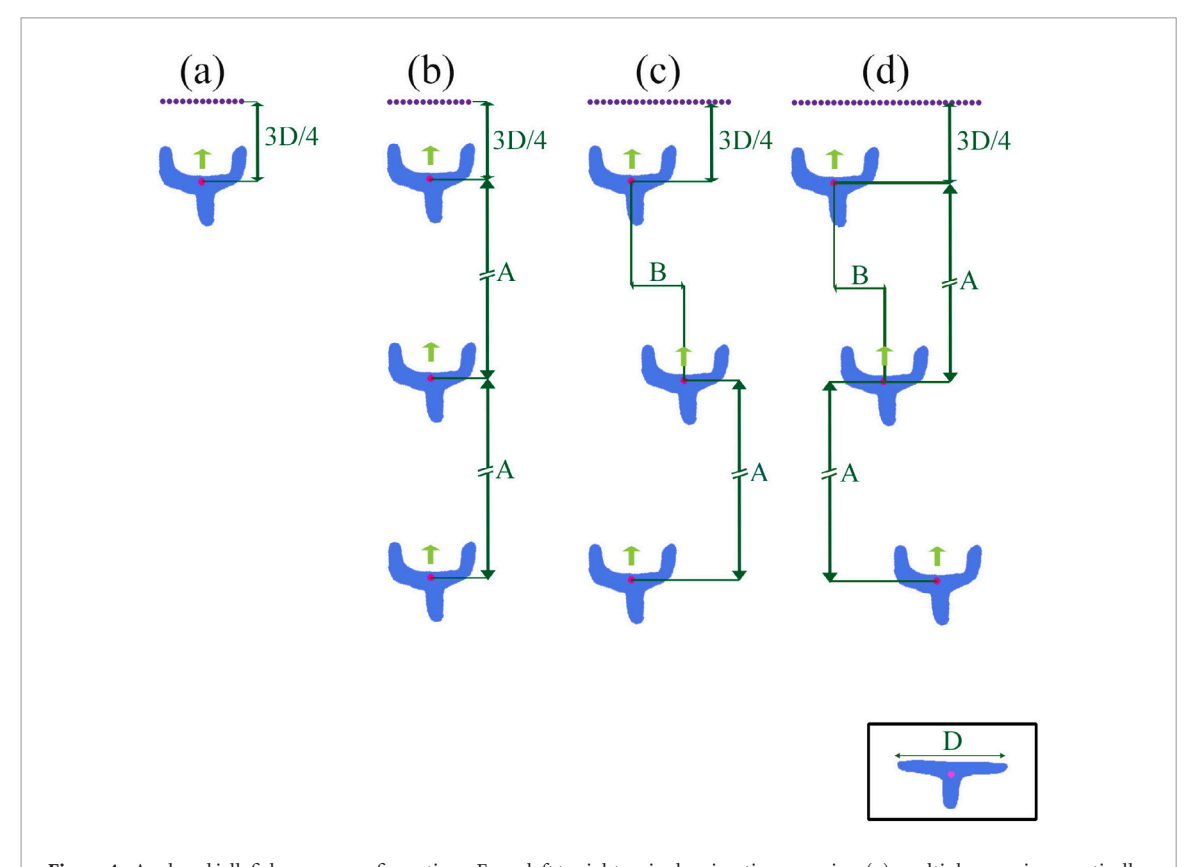


Figure 4. Analyzed jellyfish swarm configurations. From left to right: a single migrating organism (a), multiple organisms vertically migrating in a line (b), multiple organisms migrating in a two-column staggered formation (c), and multiple organisms migrating in a three-column staggered formation (d). Upper case letters A and B denote the inter-organism vertical and horizontal spacings, respectively. The sketch inside the black outlined box at the bottom right corner indicates the definition of one body diameter $D=7.3\pm0.02$ mm.

Table 1. Vertical and horizontal inter-organism spacings considered in migrating swarm studies.

| Buoyancy frequency | $N = 10^{-3} \mathrm{s}^{-1}$ | | | $N = 0 \text{ s}^{-1}$ | | |
|---------------------|--------------------------------|-----|-----|------------------------|-----|----|
| Vertical spacing | 8 | D | 4D | | 8D | 4D |
| Horizontal spacing | <i>D</i> /2 | D/4 | D/2 | D/4 | D/2 | |
| Number of organisms | 38 | | 38 | | 38 | |

stratified fluid). Finally, an additional set of simulations of steady swimmers in a purely viscous regime was also performed to discuss the effect of viscosity. To this end, a regularized Stokeslet model was implemented using the same group configuration (details of the model can be found in the Appendix). Simulation parameters for the hybrid model cases are summarized in table 1.

Fluid transport was quantified by continuously tracking the position of 1000 fluid particles. In each case, the particle batch was initialized as a horizontal row positioned just above the cropped box containing the velocimetry data (3*D*/4 above the centroid of the first swimmer in a swarm). The particle row length was set to match the characteristic length scale of the aggregation, such that the non-dimensional length ratio of particle distribution length to formation span length remained constant and equal to one regardless of swimmer configuration.

Each swimmer was allowed to migrate vertically by subsequently introducing the series of cropped velocity fields at a vertical position set by the displacement of the jellyfish centroid for the duration of the three strokes of acquired PIV data. Once the last instantaneous velocity field of the third acquired stroke was introduced, the first cropped velocity field from the measurement series was inserted at the same vertical position to simulate a longer vertical swimming trajectory. In all configurations, vertical migration was simulated until the centroid of the first swimmer in the aggregation had translated 300 bell diameters from its starting position.

2.5. Particle advection scheme

In non-stratified fluid, the instantaneous position of each fluid particle was computed from the time series of velocity field measurements. To this end, the forward Euler method was implemented with a time step set by the PIV image acquisition rate ($\Delta t = 0.033$ s) to solve:

$$\frac{d\mathbf{x}}{dt} = \mathbf{u}(\mathbf{x}), \quad \mathbf{x}(0) = \mathbf{x}_0, \tag{2}$$

where $\mathbf{u}(\mathbf{x})$ was computed via linear interpolation of the measured velocity field at each particle position, and \mathbf{x}_0 is the initial position of the particle row.

In the limit of small density variations, the effect of buoyancy on fluid transport was considered by incorporating an effective restoring velocity (assuming critically damped dynamics) acting only in the vertical direction [19, 26]:

$$\mathbf{u}_b = -N\left\{ (\mathbf{x} - \mathbf{x}_0) \cdot \mathbf{e}_{\mathbf{y}} \right\} \mathbf{e}_{\mathbf{y}},\tag{3}$$

where gravity acts along the $-\mathbf{e}_y$ direction. Fluid transport in a homogeneous water column was hence estimated using equation (2), whereas equations (2) and (3) were combined so that fluid is advected by $\mathbf{u}(\mathbf{x}) + \mathbf{u}_b(\mathbf{x})$ to account for a weak linear stratification. The assumption of negligible production of baroclinic vorticity is justified in this case given that local density perturbations remain within the limit of $ND/U \ll 1$.

3. Results

3.1. Single swimmer

In contrast to steady self-propelled swimmers, *A. aurita* generates thrust via periodic bell contraction-and-relaxation cycles that induce a complex vortex structure in the wake [24]. PIV data analysis of the three swimming cycles implemented in the numerical model demonstrated the generation of sequential starting and stopping vortices during the power and recovery strokes, respectively (figure 5). It was observed that as the organism swam toward the initially uniformly distributed particle row, fluid particles were quickly engulfed by the wake and predominantly advected near the body along the jellyfish swimming direction (Supplementary Video 1 (stacks.iop.org/BB/15/015002/mmedia)).

The effect of vortex interactions on near-field transport is two-fold: (a) all particles are advected from their equilibrium position, and (b) the initially horizontally oriented particle batch is re-distributed along the axis of the swimmer. These effects can be observed in figure 6, which shows the position of the particle batch during vertical migration in both a homogeneous and a weakly stratified fluid environment. Similar distributions can be appreciated in fields derived from velocimetry data of other jellyfish species, but not in idealized flow models (i.e. [20] and [19], respectively).

As the ephyra reached eight body diameters of travel, particles in the homogeneous fluid were vertically displaced up to 6.31 body diameters from their starting position and up to 5.6 body diameters considering $N=10^{-3}\,\mathrm{s}^{-1}$ (figure 7). The drift volume V_D defined as the volume of fluid comprised between the surface coincident with the equilibrium position of the particle row and the one delineated by the position of the particles at a given time was computed according to [27]:

$$V_D = 2\pi \int_0^R yr dr , \qquad (4)$$

where y corresponds to the instantaneous vertical position of the fluid particles, r the distance from the swimmer projected in the xz plane, and R is set by the maximum horizontal spread of the particle batch (radius of the material surface) at a given time.

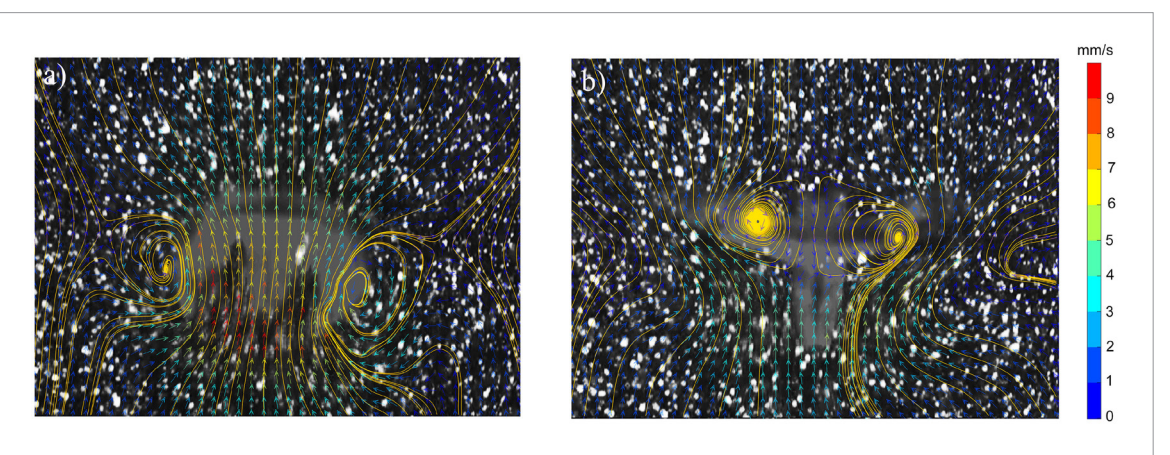


Figure 5. Swimming kinematics. Velocity fields and streamlines show starting (a) and stopping (b) vortices produced during power and recovery, respectively. Raw PIV data is superimposed for reference.

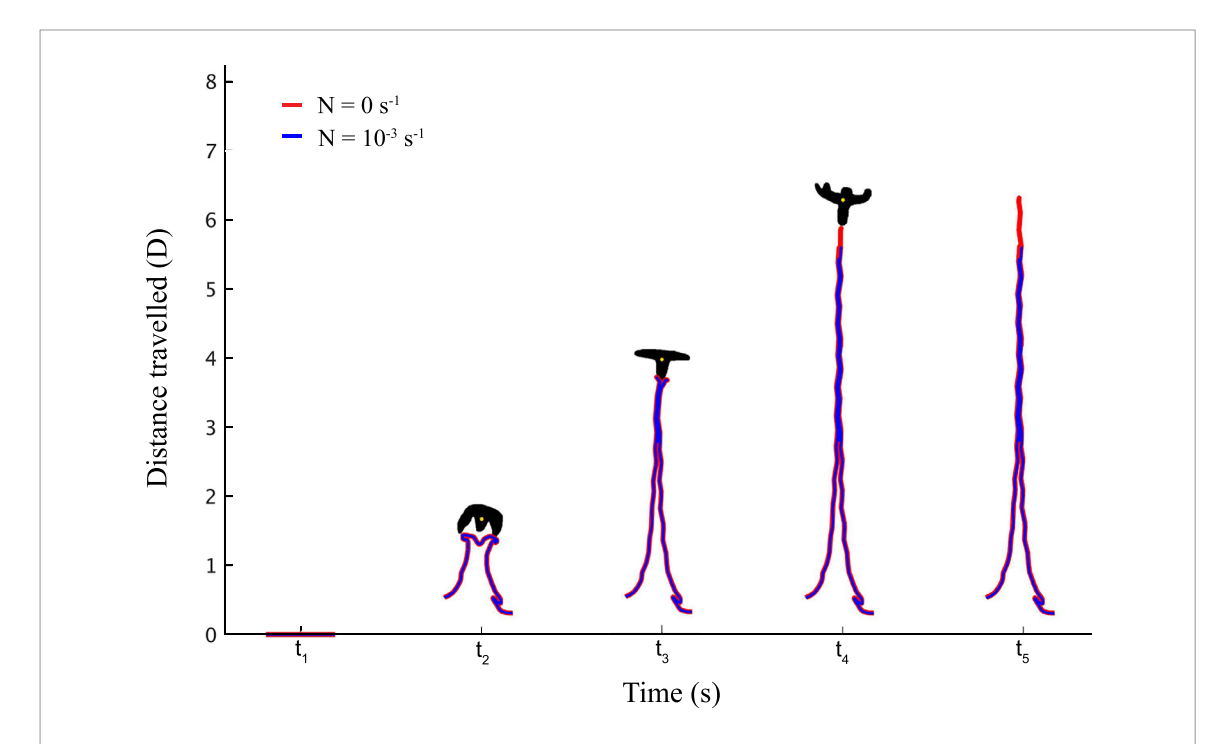


Figure 6. Advection of a fluid particle row due to vertical migration of a single swimmer. The instantaneous position of the organism and that of the simulated fluid particles are shown at different instants during the simulation ($\Delta t = 4$ s). Each time stamp coincides with the initial horizontal position of the center of mass of the particle batch. The reader is referred to Supplementary Video 2 for the complete series.

Initially, as the organism migrates vertically, the particle batch is continuously rearranged as fluid particles follow looping trajectories that position them closer to the jellyfish body axis resulting in an increase of the drift volume with respect to time (i.e. t_2 and t_3 in figure 6). The volume of the jellyfish ($V_J = 34 \pm 1 \text{ mm}^3$) was calculated from a contour image showing the bell fully extended. This value was then used to normalize the drift volume:

$$V_D^* = \frac{V_D}{V_I} \ . \tag{5}$$

In homogeneous fluid, it was found that once the organism stops interacting with the simulated particles, V_D^* converges to a constant value of 3.23, while in the presence of a weak stratification the drift volume continuously decreases due to the restoring

effect of buoyancy. Nevertheless, the volume drifted in stratified flow at the time maximum transport has been achieved in homogeneous fluid is still slightly three times greater than the volume of the jellyfish ($V_D^*=3.17$). This supports the assumption that the effect of buoyancy is minimal and does not significantly inhibit fluid transport in the vertical direction.

Comparison of these results with those obtained for *Phyllorhiza* sp. in a recent study by Katija [20] highlights the important effect of morphology on fluid transport as well as the Reynolds number dependence of the induced vertical drift. Normalized drift volumes for *Phyllorhiza* sp. with and without oral arms in homogeneous fluid were reported to reach 1.4 and 2.53, respectively. The swimming mode of the medusae studied by Katija [20] and the ephyra analyzed here is the same, but the morphology and size differ.

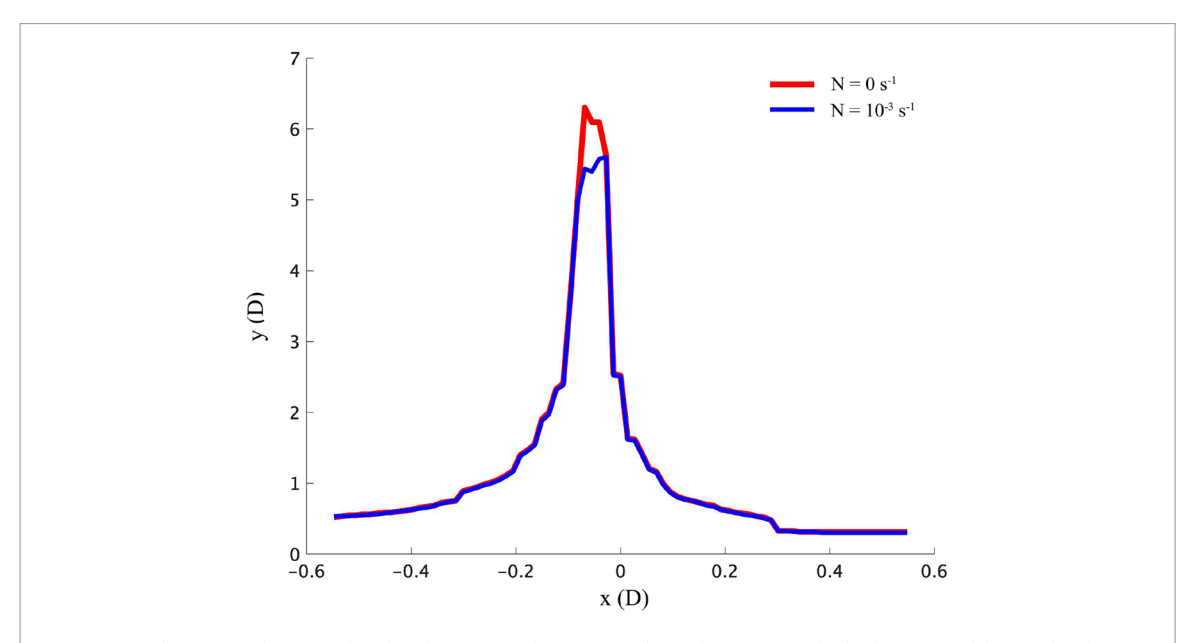


Figure 7. Deformation of a material surface due to vertical migration of a single swimmer. The final position of the simulated particle row after the organism had reached 8 body diameters of travel is shown for homogeneous and non-stratified fluid.

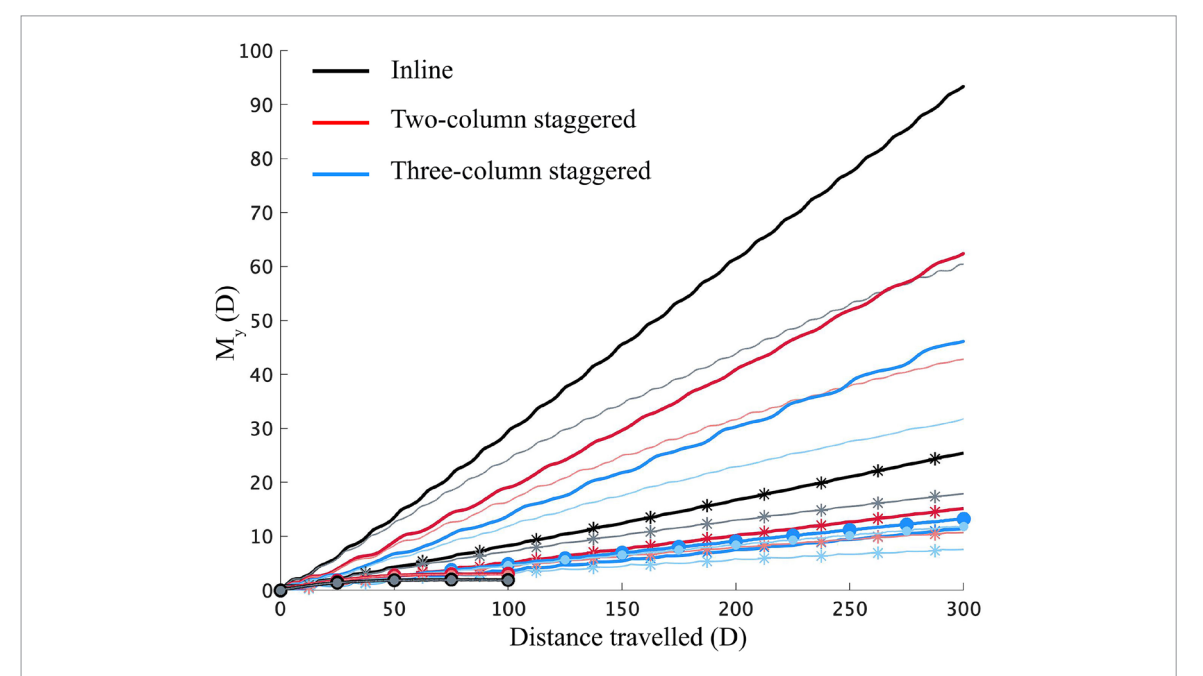


Figure 8. Mean vertical drift for different group configurations matching vertical inter-organism spacing to maximum vertical transport achieved by an individual swimmer. The vertical displacement of the centroid of the particle batch is plotted as a function of the diameters traveled by the first swimmer in the group. Simulation results in homogeneous (thick lines) and weakly stratified (thin lines) fluid are presented for the hybrid model (-), Stokeslet dipole model (*), and the dragged-sphere model in inviscid flow by Dabiri [19] (o). Note that the inline and two-column staggered cases in the simulations by Dabiri [19] converge to a constant value after 100 diameters of travel.

Both factors are expected to alter the drift volume. In particular, oral arms interact with the vortices at the wake, producing a different wake structure than the observed for the ephyra and the medusa without oral arms. Furthermore, the ephyra used in this study is an order of magnitude smaller (Re = 30) than the ones used by Katija (Re = 200 and Re = 730 for *Phyllorhiza* sp. with and without oral arms, respectively). This also explains why the value of the drift volume is higher for *A. aurita*, as viscosity has been shown to enhance vertical transport [3].

3.2. Jellyfish swarms

Vertical fluid transport due to a sparse group of swimmers was quantified in terms of the mean drift of the simulated particle batch, which is given by the vertical displacement of the center of mass of the batch relative to its equilibrium position [28]:

$$M_{y}(t) = \frac{1}{N_{p}} \sum_{n=1}^{N_{p}} (y_{n}(t) - y_{n}(0))$$
, (6)

where N_p is the total number of particles, $y_n(t)$ is the vertical position of a given particle n at instant t, and

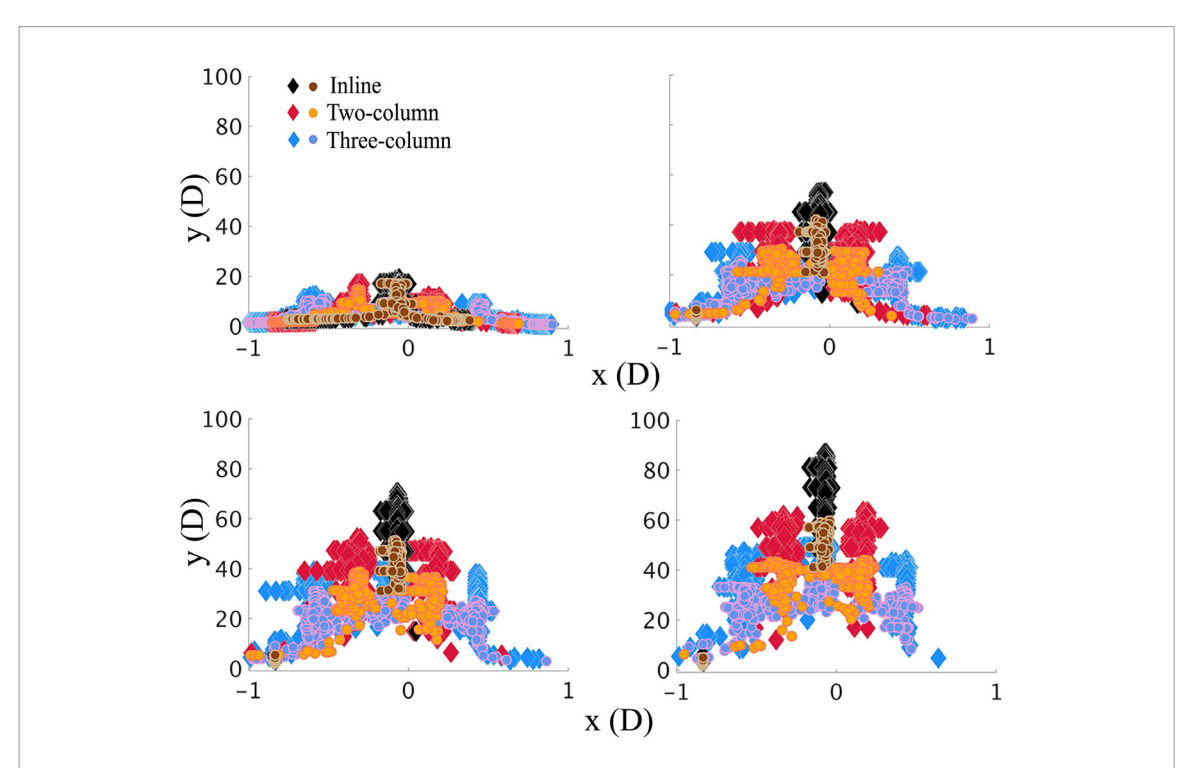


Figure 9. Particle distribution during vertical group migration. A series of snapshots show the positions of the simulated fluid particles as the first swimmer in the migrating group has traveled 50, 150, 250, and 300 body diameters (from left to right, top to bottom) in homogeneous (\Diamond) and weakly stratified ($^{\circ}$) fluid.

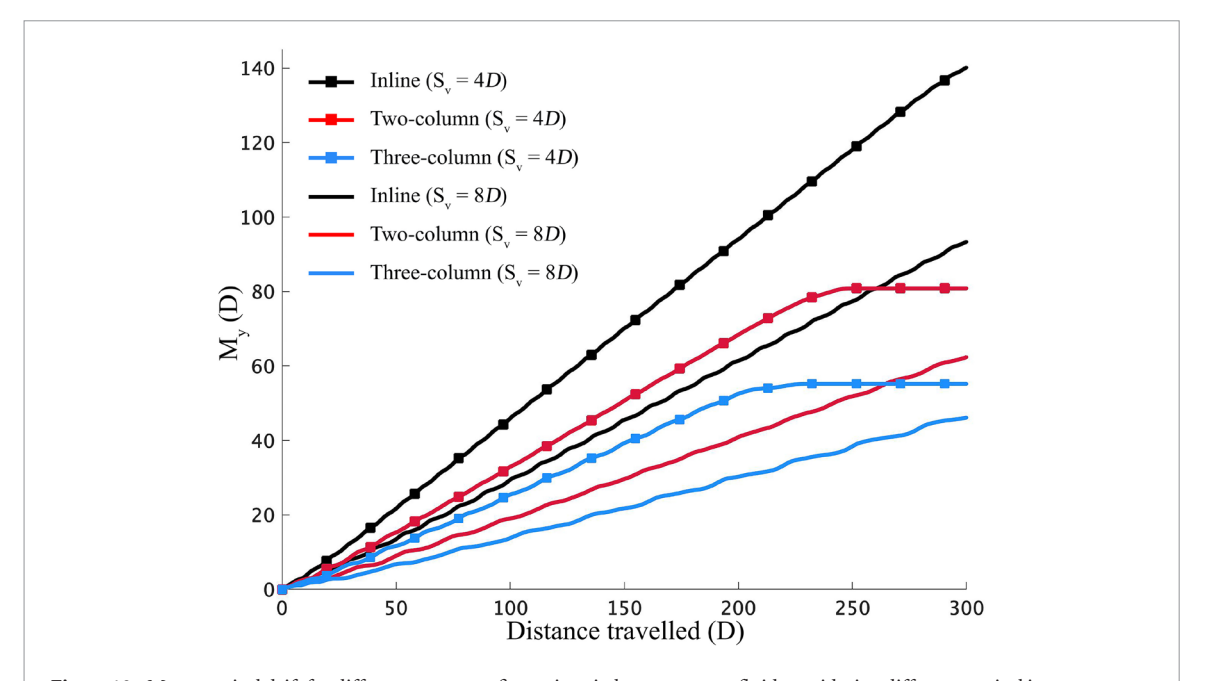


Figure 10. Mean vertical drift for different group configurations in homogeneous fluid considering different vertical interorganism spacings. The vertical displacement of the centroid of the particle batch is plotted as a function of the diameters traveled by the first swimmer in the group.

 $y_n(0)$ denotes the equilibrium position. As quantified, the mean drift implicitly depends on the initial particle configuration, which is here fixed to be a 1D row spanning the horizontal span of the aggregation. This metric is shown in figure 8 as a function of the distance traveled by the first swimmer in the aggregation considering both fluid scenarios for an inline, two-column and three-column staggered aggregations (considered vertical and horizontal inter-organism spacings were 8D and D/2, respectively). Results

from the potential flow model by Dabiri [19] and a regularized Stokeslet model (Appendix) are also plotted for reference.

As expected, advection of the particle batch by our hybrid numero-experimental model occurred on much greater length scales than by a rigid sphere with a momentumless wake translating in an idealized fluid. A notable difference from potential flow predictions [19] is that vertical fluid transport is maximized for an inline group configuration rather than for a

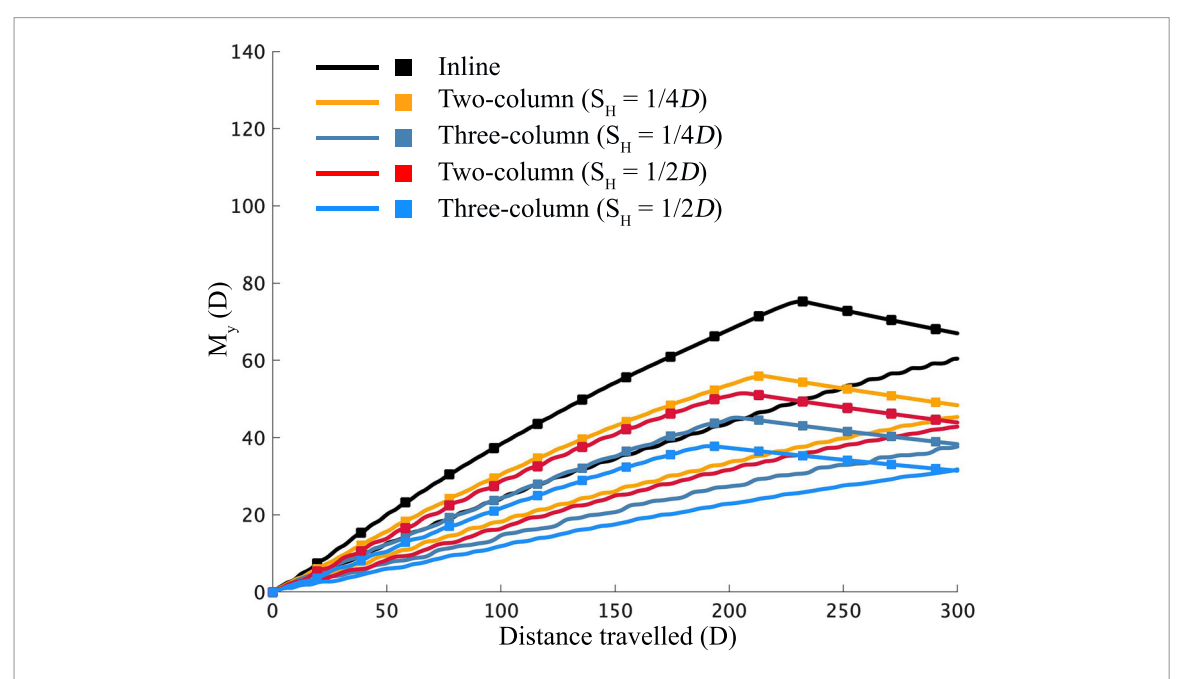


Figure 11. Mean vertical drift for different group configurations in weakly stratified fluid. Results are shown for aggregations with vertical inter-organism spacing of 8D (solid lines) and 4D (lines with markers). Horizontal inter-organism spacing is denoted in the legend.

two- or three-column staggered swarm. In particular, the production of vortex rings near the bell effectively traps fluid particles near the jellyfish body and drags them with it as the bell relaxes. Due to the continuous production of vortex rings as the organism swims forward, fluid particles are vertically advected on length scales much greater than an organism body length and are horizontally distributed in the vicinity of the body axis (Supplementary Videos 3, 4 and 5). In the case of a solid sphere vertically translating in potential flow, the absence of vortex rings in the wake of the object results in a wider particle distribution perpendicular to the swimming direction, thus favoring a staggered formation over one in line for maximum vertical transport (see Supplementary Materials of [19]).

Results obtained using aggregations of regularized Stokeslet dipoles yielded greater vertical transport than corresponding cases in inviscid fluid, but still underestimated the net amount achieved by real swimmers regardless of the configuration of the swarm. On short migration time scales (such that only the first swimmer in the aggregation is interacting with the particle row), the Stokes swimmers effectively advected fluid particles beyond the maximum achievable distance by the hybrid model (7.6D compared to 6.3D, after 8D of travel). However, due to the diffuse nature of the vorticity field produced by the Stokes multipole solution, particles were also advected opposite to the swimming direction. Although reflux flows have been observed in other jellyfish species (e.g. [20]), A. aurita was not observed to generate any backward transport. In any case, as fluid is displaced from the equilibrium position, reflux also contributes to mixing. However, its contribution is weaker than transport in the direction of travel, ultimately leading to lesser vertical transport

Table 2. Standard deviation of final particle displacements in the horizontal direction for all configurations: inline, two-column (2C) and three-column staggered (3C). Vertical and horizontal interorganism spacings are denoted by S_V and S_H , respectively.

| Final horizontal spread about th | ne center of | f mass (D |)) |
|----------------------------------------------------|--------------|-----------|------|
| Configuration parameters | Inline | 2C | 3C |
| $N = 0 \text{ s}^{-1}, S_V = 8D, S_H = D/2$ | 0.01 | 0.27 | 0.47 |
| $N = 0 \text{ s}^{-1}, S_V = 4D, S_H = D/2$ | 0.02 | 0.30 | 0.45 |
| $N = 10^{-3} \text{ s}^{-1}, S_V = 8D, S_H = D/2$ | 0.02 | 0.28 | 0.42 |
| $N = 10^{-3} \mathrm{s}^{-1}, S_V = 8D, S_H = D/4$ | 0.02 | 0.25 | 0.29 |
| $N = 10^{-3} \mathrm{s}^{-1}, S_V = 4D, S_H = D/2$ | 0.02 | 0.27 | 0.48 |
| $N = 10^{-3} \text{ s}^{-1}, S_V = 4D, S_H = D/4$ | 0.02 | 0.28 | 0.28 |
| | | | |

as more swimmers are set to interact with the particle batch (Supplementary Videos 4, 5 and 6).

Due to the interplay of organism morphology and swimming mode, A. aurita draws fluid towards its body axis and leaves a vertical trail of particles closely aligned to this position as it swims. As a result, swarm configurations with swimmers propelling in line always encounter particles to advect, whereas aggregations formed by alternating swimmers spread fluid perpendicular to the swimming direction and thus transport less fluid upwards. This can be observed from the distribution of the particle batch at different stages of a migration event (figure 9). In both simulated fluid scenarios, vertical transport is maximized for jellyfish swarms that effectively minimize spreading fluid in the horizontal direction. This effect is also captured in the low-order Stokes simulations, whereby the presence of vorticity together with the governing dipole solution enhances the advection of fluid close to the axis of travel of the regularized singularity. Therefore, an inline formation results in maximum net vertical transport compared to the other configurations.

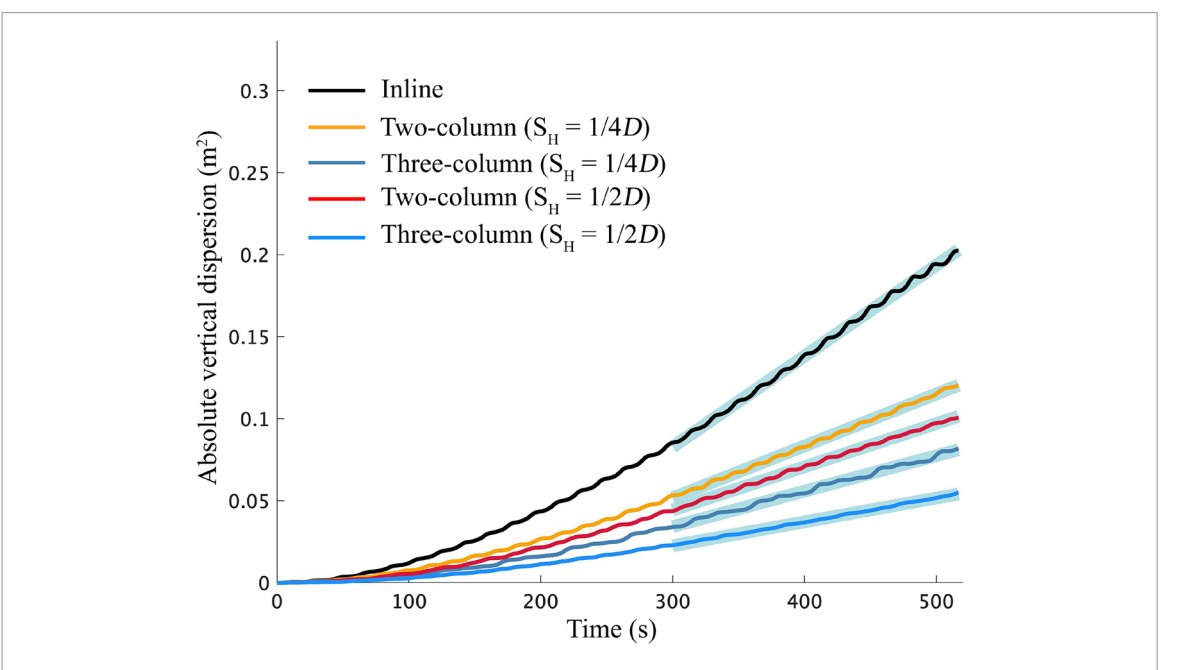


Figure 12. Absolute vertical dispersion for configurations with a vertical inter-organism spacing of 8*D* in weakly stratified fluid. Horizontal inter-organism spacing is denoted in the legend. The shaded regions indicate the linear fit used to quantify a vertical stirring coefficient.

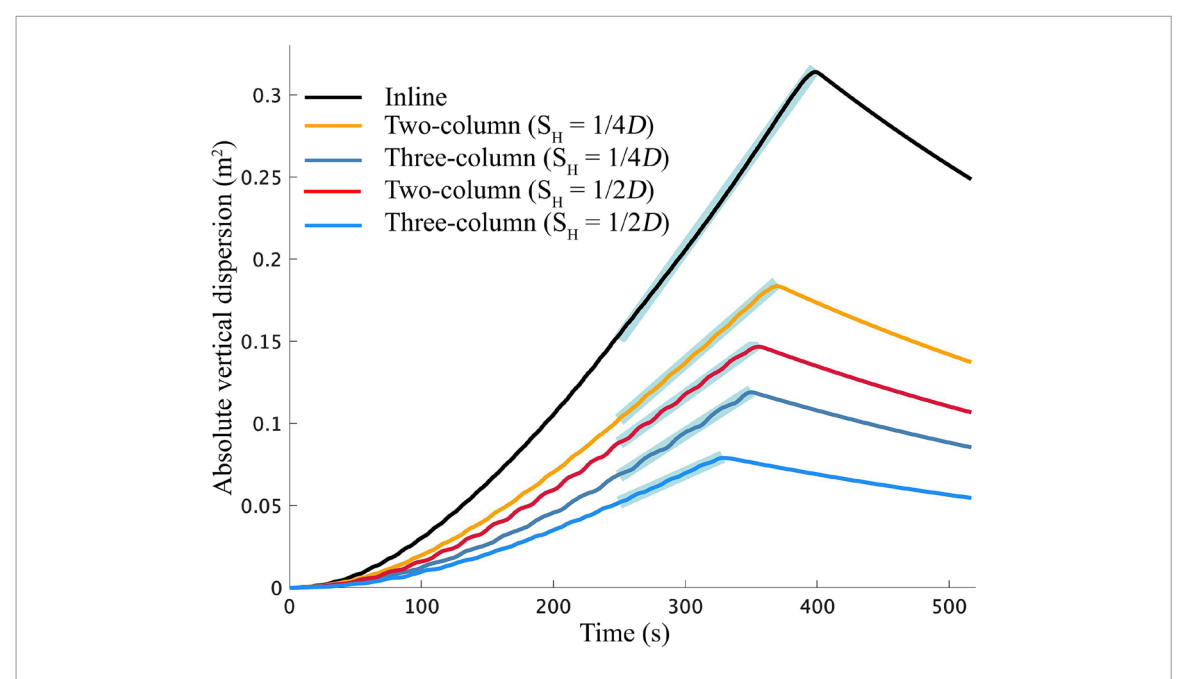


Figure 13. Absolute vertical dispersion for configurations with a vertical inter-organism spacing of 4D in weakly stratified fluid. Horizontal inter-organism spacing is denoted in the legend. The shaded regions indicate the linear fit used to quantify a vertical stirring coefficient.

The disagreement in the net amount of vertical fluid transport between the hybrid and Stokes models can be explained by looking at the time-dependence of each flow and its effect on particle trajectories. The unsteady nature of the wake induced by real swimmers results in effective entrainment and trapping of fluid particles, compared to the steady flow produced by the swimmer in Stokes flow (compare Supplementary Videos 3, 4, and 5 to 6, 7, and 8).

The effect of vertical inter-organism spacing on vertical fluid transport was analyzed by reducing the vertical distance between neighboring organisms by 50% while

keeping the number of organisms in a swarm constant (table 1). Overall, in homogeneous fluid, reducing the spacing between consecutive swimmers in a group from 8 to 4 body diameters resulted in a considerable increase of the mean vertical drift (figure 10). In particular, the mean drift by the jellyfish swarm with an inline configuration was observed to increase by 50%, compared to a 30% and 20% increase for two- and three-column staggered configurations, respectively. This result is intuitive, as more organisms are allowed to interact with the particle batch for swarms with reduced vertical inter-organism spacings over the same time interval as swarms with

Table 3. Vertical stirring coefficient for all configurations: inline, two-column (2C) and three-column staggered (3C). Vertical and horizontal inter-organism spacings are denoted by S_V and S_H , respectively.

| Vertical stirring coefficient ($\cdot 10^{-4} \text{ m}^2 \text{ s}^{-1}$) | | | | | | |
|------------------------------------------------------------------------------|--------|------|------|--|--|--|
| Configuration parameters | Inline | 2C | 3C | | | |
| $S_V = 8D, S_H = 1/2D$ | 2.77 | 1.32 | 0.73 | | | |
| $S_V = 8D, S_H = 1/4D$ | | 1.58 | 1.08 | | | |
| $S_V = 4D, S_H = 1/2D$ | 5.57 | 2.90 | 1.79 | | | |
| $S_V = 4D, S_H = 1/4D$ | | 3.50 | 2.59 | | | |
| | | | | | | |

greater spacing between neighboring swimmers. In this limit, the maximum overturning length scale for the two-and three-column staggered configurations was reached near the end of the simulation (80.9 and 55.2 body diameters, respectively).

In agreement with results obtained in homogeneous fluid, simulations performed in a weakly stratified fluid environment showed that decreasing the vertical inter-organism spacing within an aggregation increases net vertical fluid transport (figure 11). In this limit, maximum over-turning length scales ranging from 75.3 to 37.8 body diameters were reached within less than 300 body diameters of travel. A subsequent decrease in vertical drift is observed as no more organisms are left to interact with the particle batch and thus fluid returns to its equilibrium position. In the case of aggregations with large vertical spacing between organisms, maximum fluid transport was not attained during the duration of the simulation.

In addition to reducing the vertical spacing between consecutive swimmers, the horizontal inter-organism spacing was also reduced by 50% for studies with two- and three-column staggered configurations in stratified fluid (also shown in figure 11). A reduction in the horizontal spacing between neighboring swimmers yielded a 9% and 20% increase in vertical transport for two- and three-column staggered cases, respectively, compared to more spread-out groups with the same configurations. Shrinking the horizontal spacing between successive swimmers increases vertical transport even more because it effectively decreases the horizontal spreading of fluid particles during a migration event.

To illustrate how spreading fluid in the direction opposite of travel affects vertical transport, the final horizontal spread about the axis of symmetry of the particle batch at its equilibrium position was quantified using the square root of the variance of the displacements in the horizontal direction (ignoring particles more than four standard deviations from the mean, see table 2). As expected, the swimmer configuration that achieved the greatest vertical transport spread particles minimally in the horizontal direction. In particular, this metric was an order of magnitude less for a group migrating in line with vertical interorganism spacing of 4D than for three-column staggered migrations with corresponding vertical interorganism spacings.

4. Discussion

4.1. Near-field flow and vertical fluid transport

Numerical simulations of jellyfish swarms with different configurations demonstrated the non-negligible effect of the near-field fluid dynamics on large-scale fluid transport during vertical migration. Unexpectedly, the aggregation that transported the greatest amount of simulated fluid particles upwards did not correspond to a multi-staggered swarm but rather one composed by a line of swimmers. A reduction of inter-organism spacing had a non-negligible impact on the amount of fluid transported upwards but did not position transport by multi-staggered swarms ahead of that acquired by a jellyfish group migrating in line.

Comparison of transport by the hybrid model to simulations set via the implementation of commonly used models for self-propelled swimmers in potential and Stokes flows highlighted the relevant transport mechanisms leveraged by real swimmers during vertical migration. In particular, for the species of jellyfish implemented in our model, a so-called starting vortex is generated near the bell at the beginning of the swimming cycle. As a result, fluid particles move in looping trajectories toward the center of the organism. Fluid entrainment persists during the recovery stroke by the subsequent production of a stopping vortex close to the body. As the organism transitions to the next swimming cycle and the bell relaxes, the fluid in the vicinity of the organism drifts along the swimming direction (Supplementary Video 2). Although the vorticity field imposed by the regularized Stokeslet model results in a better representation of the flow field compared to swimmers in the inviscid limit, neglecting the unsteadiness of the near-field produces a very different fluid particle distribution over time. Due to the combined effect of an unsteady swimming gait, morphology, and the unsteady nature of the wake of a real swimmer, the instantaneous flow in the wake is not the same as the time-integrated value. Fluid transport is thus unavoidably affected by these dynamics, and if the dispersion of fluid due to vertically migrating swimmers is of interest, these results demonstrate that the near-field of the organism cannot be neglected in the analysis.

In addition, the results obtained in this investigation were produced in the limit of dilute aggregations, such that the wakes of neighboring swimmers do not interact with each other. However, dense swarm migration events have been observed in the field, e.g. photographic records of Antarctic krill by Hamner and Hamner [13]. Based on laboratory experiments of dense migrating aggregations of A. Salina ([9] and [12], that show additional vertical transport pathways via hydrodynamic interactions between swimmers), it is expected that the results presented in this paper are an underestimate compared to the case of a densely aggregated zooplankton swarm.

4.2. Biomixing implications

Finally, the Lagrangian description can be extended to analyze the dispersion regime induced by migrating jellyfish swarms via an absolute dispersion coefficient [28]:

$$D_{y} = \frac{1}{N_{p} - 1} \sum_{n=1}^{N_{p}} (y_{n}(t) - y_{n}(0))^{2}.$$
 (7)

It was observed that, in all cases, D_y followed a parabolic behavior within the first quarter of the duration of the simulation, followed by a linear growth until maximum vertical fluid transport was achieved (figures 12 and 13). Hence, after a short transient, the variance of particle displacements relative to their equilibrium position was found to grow approximately linearly with respect to time, i.e. what is known as normal dispersion. We note that this coefficient does not characterize the spread of an initial cloud of particles, but should rather be viewed as a measure of stirring generated by the swarm. Following Taylor's analysis [29], a vertical stirring coefficient can be defined as the rate of increase of the dispersion coefficient in the vertical direction:

$$\kappa = \frac{1}{2} \frac{d}{dt} D_y \,. \tag{8}$$

Analysis of the Lagrangian statistics of the simulated swarm configurations resulted in an effective vertical stirring coefficient in the order of $O(10^{-4})\,\mathrm{m^2\,s^{-1}}$, with the maximum value achieved for an inline formation with reduced inter-organism spacing ($\kappa = 5.57 \times 10^{-4}\,\mathrm{m^2\,s^{-1}}$, see table 3). These values are within the same order of magnitude as previous predictions by Dabiri [19], supporting the claim that idealized models provide order-of-magnitude estimates.

Finally, considering that A. Aurita is commonly found above and within the thermocline [30, 31], a biomixing time scale can be computed. Above the thermocline, in the mixed ocean layer, fluid properties can be considered to be well-mixed. Within the thermocline, however, steep gradients of salinity and temperature are present. By dimensional analysis, the time it would take a jellyfish swarm to mix a section of the thermocline L_T can be estimated as $T = L_T^2/(2\kappa)$. Taking the thickness L_T to correspond to the thickness of either the diurnal or seasonal thermocline (which ranges between 1 and 10 m, respectively, depending on atmospheric forcing [32]) and the effective vertical stirring coefficient as the mean value obtained in this study, T is found to range from 35 min to 2.4 days. The time scale associated with the dynamics of physical processes at the thermocline lies within this range. Hence, our model results suggest that dilute jellyfish swarms have the potential to modify steep vertical density gradients and mix sections of the thermocline to contribute to staircase variations of density, which are commonly observed in oceanographic data [32] and recent experimental studies [33].

Acknowledgments

The authors gratefully acknowledge Caitlin Regan for her help with data acquisition, Patrice Klein for his comments on earlier versions of the manuscript, and Rachel Pepper for many discussions and advise on low-order models of self-propelled swimmers in the Stokes limit. Support for this work was provided by the Binational Science Foundation and National Science Foundation programs in Fluid Dynamics and Biological Oceanography.

Appendix. Regularized force-dipole model

To implement a low-order flow model that accounts for the presence of vorticity, we neglect unsteadiness caused by the swimming stroke and consider a constant swimming velocity U_s (equal in magnitude to the average swimming speed of the jellyfish). Denoting the swimming direction by d (so that $U_s = U_s d$), the center of mass of the swimmer is located at $\mathbf{x}_s(t) = \mathbf{x}_s(0) + U_s t$. We model the neutrally buoyant swimmer as carrying with it a force dipole along with higher-order force multipoles that make minor contributions to the flow. To circumvent the issue of resolving the swimmer boundaries, and to avoid singular velocities near the origin, we regularize the force-dipole using the formalism of [34, 35].

The fundamental solution of the regularized force multipole model satisfies the Stokes equations with a distributed body force $f(r) = F\phi(r)$ with $\phi(r) = 15a^48\pi r_a^7$, where $r = x - x_s(t)$ and $r_a = (|r|^2 + a^2)^{1/2}$ [34]. The force is distributed over the characteristic volume a^3 , where a is taken as the radius of the jellyfish bell; the limit $a \to 0$ recovers the Oseen tensor. Since the swimmer is force-free, we are interested in the force dipole, which is the gradient of the fundamental solution. Furthermore, the symmetry of the flow field induced by the self-propelled organism suggests a negligible contribution from the antisymmetric part of the force dipole in the absence of body rotations. The corresponding velocity field is then (see [35])

$$\boldsymbol{u}(\boldsymbol{r}) = \frac{1}{8\pi\mu} \left[\left(\frac{\boldsymbol{I}}{r_a^3} - \frac{3\boldsymbol{r}\boldsymbol{r}}{r_a^5} \right) : \boldsymbol{S}\boldsymbol{r} - \frac{3a^2}{r_a^5} \boldsymbol{S} \cdot \boldsymbol{r} \right],$$
(A.1)

where S is the stresslet tensor (rank-2 symmetric and traceless) and is a property of the swimmer. From our flow measurements and the associated trajectories of fluid parcels (figure 6), we infer that the jellyfish locomotes as a puller, characterized by fluid flow towards its center of mass along the swimming axis d (which in our simulations we identify with e_y). The stresslet of such a swimmer is:

$$S = -S\left(dd - \frac{I}{3}\right),\tag{A.2}$$

where *S* is the stresslet strength (positive for a puller). Equations (A.1) and (A.2) define the flow around the

swimmer. Lagrangian trajectories of passive tracers of the flow are characterized by a single dimensionless parameter,

$$S^* = \frac{S}{\mu a^2 U_s} \tag{A.3}$$

that quantifies the stresslet strength relative to the swimming speed. In our simulations, we use $S^* = 12\pi$, consistent with a dipole length of O(a)and a dipole force of $O(6\pi \mu a U_s)$ (which assumes that deformations of the swimmer body are comparable with the swimming speed). An alternative is to infer S* from the drift volume, as analyzed by [17] under both the Stokes and Oseen approximations for the flow, albeit without the regularization employed here. Their work suggests $V_D^* = O(2S^*/Re)$, which for our parameters yields a value of $S^* = O(40)$ (close to the value chosen in our simulations). A systematic study of drift volumes under regularized Stokes and Oseen approximations is warranted and may prove to be a useful way to quantify transport by the near-field flows of swimmers.

ORCID iDs

M M Wilhelmus https://orcid.org/0000-0002-3980-2620

J Nawroth https://orcid.org/0000-0003-1898-3968 B Rallabandi https://orcid.org/0000-0002-7733-8742

References

- [1] Katija K 2012 Biogenic inputs to ocean mixing *J. Exp. Biol.* 215 1040–9
- [2] Breitburg D L, Crump B C, Dabiri J O and Gallegos C L 2010 Ecosystem engineers in the pelagic realm: alteration of habitat by species ranging from microbes to jellyfish *Int. Comput. Biol.* 50 188–200
- [3] Katija K and Dabiri J O 2009 A viscosity-enhanced mechanism for biogenic ocean mixing *Nature* **460** 624–6
- [4] Rousseau S, Kunze E, Dewey R, Bartlett K and Dower J 2010 On turbulence production by swimming marine organisms in the open ocean and coastal waters J. Phys. Oceanogr. 40 2107–21
- [5] Rippeth T P, Gascoigne J C, Green J A M, Inall M E, Palmer M R, Simpson J H and Wiles P J 2007 Turbulent dissipation of coastal seas Sci. Electron. Lett. a 1
- [6] Kunze E, Dower J F, Beveridge I, Dewey R and Bartlett K P 2006 Observations of biologically generated turbulence in a coastal inlet Science 313 1768–70
- [7] Dean C, Soloviev A, Hirons A, Frank T and Wood J 2016 Biomixing due to diel vertical migrations of zooplankton: Comparison of computational fluid dynamics model with observations Ocean Model 98 51–64
- [8] Noss C and Lorke A 2014 Direct observation of biomixing by vertically migrating zooplankton *Limnol Oceanogr.* 59 724–32
- [9] Wilhelmus M M and Dabiri J O 2014 Observations of largescale fluid transport by laser-guided plankton aggregations *Phys. Fluids* 26 101302

- [10] Visser AW 2007 Biomixing of the oceans? Science 316 838-9
- [11] Wagner G L, Young W R and Lauga E 2014 Mixing by microorganisms in stratified fluids *J. Mar. Res.* **72** 47–72
- [12] Houghton I A, Koseff J R, Monismith S G and Dabiri J O 2018 Vertically migrating swimmers generate aggregation-scale eddies in a stratified column *Nature* 556 497–500
- [13] Hamner W M and Hamner P P 2000 Behavior of Antarctic krill (Euphausia superba): school, foraging, and antipredatory behavior Can. J. Fish Aquat. Sci. 57 192–202
- [14] Ardekani A M and Stocker R 2010 Stratlets: low Reynolds number point-force solutions in a stratified fluid *Phys. Rev.* Lett. 105 084502
- [15] Leshansky A M and Pismen L M 2010 Do small swimmers mix the ocean? *Phys. Rev.* E **82** 025301(R)
- [16] Subramanian G 2010 Viscosity-enhanced bio-mixing of the oceans Curr. Sci. 98 1103–8 (https://www.jstor.org/ stable/24111768)
- [17] Chrisholm N G and Khair A S 2018 Partial drift volume due to a self-propelled swimmer *Phys. Rev. Fluids* 3 014501
- [18] Wang S and Ardekani A M 2015 Biogenic mixing induced by intermediate Reynolds number swimming in stratified fluids Sci. Rep. 5 17448
- [19] Dabiri J O 2010 Role of vertical migration in biogenic ocean mixing Geophys. Res. Lett. 37 L11602
- [20] Katija K 2015 Morphology alters fluid transport and the ability of organisms to mix oceanic waters *Integr. Comput. Biol.* 55 698–705
- [21] Nawroth J C, Lee H, Feinberg A W, Ripplinger C M, McCain M L, Grosberg A, Dabiri J O and Parker K K 2012 A tissue-engineered jellyfish with biomimetic propulsion *Nat. Biotechnol.* 30 792–7
- [22] Park S J et al 2016 Phototactic guidance of a tissue-engineered soft-robotic ray *Science* 353 158–62
- [23] Raffel M, Willert CE, Wereley S and Kompenhans J 2007 Particle Image Velocimetry (Berlin: Springer)
- [24] Dabiri J O, Colin S P, Costello J H and Gharib M 2005 Flow patterns generated by oblate medusan jellyfish: field measurements and laboratory analyses J. Exp. Biol. 208 1257–65
- [25] Wunsch C and Ferrari R 2004 Vertical mixing, energy, and the general circulation of the oceans *Annu. Rev. Fluid Mech.*
- [26] Vallis G K 2006 Atmospheric and Oceanic Fluid Dynamics (Cambridge: Cambridge University Press)
- [27] Eames I 2003 The concept of drift and its application to multiphase and multibody problems *Phil. Trans. R. Soc.* A 361 2951–65
- [28] LaCasce J H 2008 Statistics from Lagrangian observations *Prog. Oceanogr.* 77 1–29
- [29] Taylor G I 1921 Diffusion by continuous movements *Proc. Lond. Math. Soc.* 20 196–212
- [30] Mutlu E 2001 Distribution and abundance of moon jellyfish (*Aurelia aurita*) and its zooplankton food in the Black Sea *Mar. Biol.* **138** 329–39
- [31] Malej A, Turk V, Lučić D and Benović A 2007 Direct and indirect trophic interactions of *Aurelia* sp. (Scyphozoa) in a stratified marine environment (Mljet Lakes, Adriatic Sea) *Mar. Biol.* **151** 827–41
- [32] Price J F and Weller R A 1986 Diurnal cycling: observations and models of the upper ocean response to diurnal heating, cooling, and wind mixing *J. Geophys. Res.* **91** 8411–27
- [33] Houghton I A and Dabiri J O 2019 Alleviation of hypoxia by biologically generated mixing in a stratified water column *Limnol Oceanogr.* 64 2161–71
- [34] Cortez R, Fauci L and Medovikov A 2005 The method of regularized Stokeslets in three dimensions: analysis, validation, and application to helical swimming *Phys. Fluids* 17 031504
- [35] Cortez R and Varela D 2015 A general system of images for regularized Stokeslets and other elements near a plane wall *J. Comput. Phys.* **285** 41–54